# 11

# Superspace Group Approach to the Crystal Structure of Thermoelectric Higher Manganese Silicides $MnSi_\gamma$

Yuzuru Miyazaki
*Department of Applied Physics, Graduate School of Engineering, Tohoku University*
*Japan*

## 1. Introduction

Thermoelectric (TE) materials directly convert waste heat into electricity based on the Seebeck effect. This process itself yields no extra gas, noise, or vibration, and it is thus recognized as a clean power generator for next decades. Currently, large amounts of waste heat, ranging from $<$100 °C (PCs, TVs, etc.) to $\sim$1000 °C (power stations, incinerators, etc.), are emitted into the environment, but some of which can be recovered as electricity by simply placing TE materials on the waste heat sources. Of the waste heat, exhaust gases from automobiles account for a total energy of 460 Pcal (4.6 $\times 10^{17}$ cal) per year in Japan (Terasaki, 2003) and if we can recover 10% of this energy, the total generated electricity would equate to that of a typical thermal power station.

TE generators usually consist in series of $\sim$100-pair p-n junctions of TE materials. The performance of TE materials is commonly evaluated by the "figure-of-merit" using the Seebeck coefficient $S$, electrical conductivity $\sigma$, and thermal conductivity $\kappa$ as $Z = S^2\sigma/\kappa$. We also use the dimensionless figure-of-merit $ZT$ ($T$ the absolute temperature) and the "power factor" given by $S^2\sigma$. For good characteristics in a TE material, a large $S$ and $\sigma$ as well as a small $\kappa$ are necessary although all three parameters are dependent on carrier concentration and hence are correlated. The best TE materials are to be found in doped-semiconductors as the Seebeck coefficient is significantly smaller in conventional metals. A $ZT$ value larger than unity is regarded as a measure of practical application because it roughly corresponds to a thermal-to-electric conversion efficiency of $\eta\sim$10 %. However, $\eta>$10 % can be achieved at higher operating temperatures above 600 K even if $ZT<1$.

Since the 1960's, higher manganese silicides (HMSs) have been extensively studied as potential p-type thermoelectric materials both in Russia and Japan (Nikitin et al., 1969; Nishida, 1972). The compounds exhibit $ZT$ = 0.3-0.7 at around 800 K (Fedorov & Zaitsev, 2006), but different structure formulae, e.g., $Mn_4Si_7$ (Gottlieb et al., 2003), $Mn_{11}Si_{19}$ (Schwomma et al., 1963; 1964), $Mn_{15}Si_{26}$ (Flieher et al., 1967; Knott et al., 1967), $Mn_{27}Si_{47}$(Zwilling & Nowotny, 1973), were proposed as HMS phases. Figure 1 shows the crystal structures (Momma & Izumi, 2008) of the first three of these; all three have great resemblance apart from the $c$-axis length. Until recently, controversy existed as to whether the compounds were an identical phase or a series of phases with different structures. The existence of $Mn_7Si_{12}$, $Mn_{19}Si_{33}$ and $Mn_{39}Si_{68}$ was also reported but these phases were

only recognized in a microscopic domain observed using transmission microscopy (Ye & Amelinckx, 1986). In contrast to the existence of several phases, there is only one line compound, $Mn_{11}Si_{19}$, in the Mn-Si binary phase diagram near the corresponding composition (Okamoto, 1991).

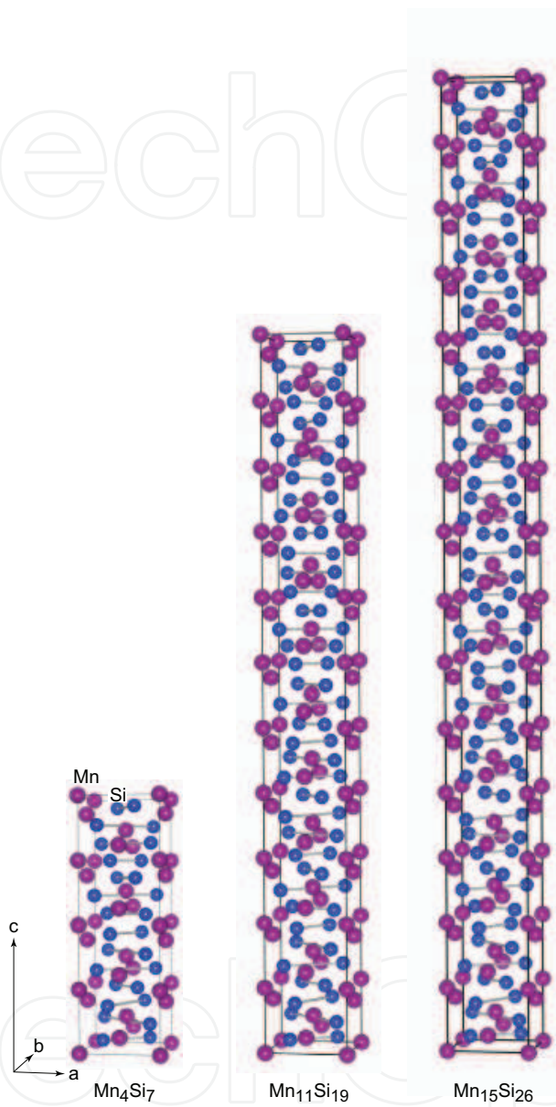


Fig. 1. Crystal structure of commensurate HMSs; $Mn_4Si_7$ ($c\sim$ 1.75 nm), $Mn_{11}Si_{19}$ ($c\sim$ 4.81 nm) and $Mn_{15}Si_{26}$ ($c\sim$ 6.53 nm).

Based on the observed electron diffraction patterns, Ye and Amelinckx (Ye & Amelinckx, 1986) proposed that the HMS phases are composed of two tetragonal basic units of Mn and Si, with an identical *a*-axis but different *c*-axes. With this idea, a variety of complicated superlattice reflections can be well indexed based on the two basic units distinguished by *c*-axis lengths, $c_{Mn}$ and $c_{Si}$. Yamamoto (Yamamoto, 1993) employed the concept of superspace group (De Wolff, 1974) to appropriately describe the detailed crystal structure of HMSs. He proposed that the HMSs belong to a family of "composite crystals", consisting of two tetragonal subsystems of [Mn] and [Si]. By means of neutron diffraction data, Miyazaki et

al (Miyazaki, 2008) succeeded in determining the detailed modulated structure using this superspace group approach. In this chapter, we describe the method by which the structure of such a composite crystal is determined based on the superspace group formalism.

## 2. Superspace group approach

### 2.1 Backgrounds

Suppose we have a crystal consisting of two tetragonal basic unit cells (i.e., subsystems) of [Mn] and [Si] with a common $a$-axis but different $c$-axes, $c_{Mn}$ and $c_{Si}$ as shown in Fig. 2. If the ratio $c_{Mn}$:$c_{Si}$ can be expressed as simple integers, such as 2:1, 3:2, etc., the whole crystal structure can be represented by a three dimensional (3D) unit cell with $c = m \times c_{Mn} = n \times c_{Si}$ ($m$ and $n$ are integers) and we no longer need to assume two basic units. The three HMSs shown in Fig. 1 are examples of such commensurate structures of $Mn_mSi_n$, although rather complicated ones. In contrast, if the $c_{Mn}$:$c_{Si}$ ratio is irrational, we then have to assume a unit cell with an infinite length along the $c$-axis. In such cases, the number of atomic sites grows too large and structural analysis becomes practically impossible. The concept of superspace group is the best way to accurately describe such a structure (De Wolff, 1974; Janner & Janssen, 1980).

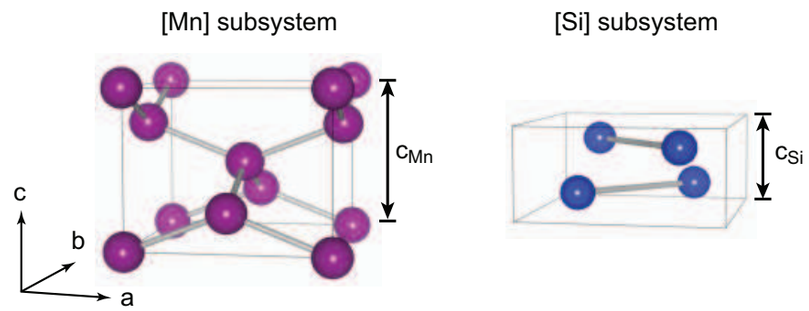


Fig. 2. Two tetragonal subsystems of [Mn] (left) and [Si] (right) with a common $a$-axis but different $c$-axis lengths, $c_{Mn}$ and $c_{Si}$.

### 2.2 General description of composite crystals

To apply the superspace group approach, we need to introduce a (3+1)-dimensional unit vectors, $\mathbf{a_{s1}}$, $\mathbf{a_{s2}}$, $\mathbf{a_{s3}}$, and $\mathbf{a_{s4}}$. Using the 3D unit bases and another $\mathbf{d}$, perpendicular to this 3D space, the relationship between these basis sets can be defined as,

$$\begin{pmatrix} \mathbf{a_{s1}} \\ \mathbf{a_{s2}} \\ \mathbf{a_{s3}} \\ \mathbf{a_{s4}} \end{pmatrix} = \begin{pmatrix} 1 & 0 & 0 & -\alpha \\ 0 & 1 & 0 & -\beta \\ 0 & 0 & 1 & -\gamma \\ 0 & 0 & 0 & 1 \end{pmatrix} \begin{pmatrix} \mathbf{a} \\ \mathbf{b} \\ \mathbf{c} \\ \mathbf{d} \end{pmatrix} \tag{1}$$

where $\mathbf{k} = (\alpha\beta\gamma)$ is a modulation vector to index the electron diffraction patterns. For the HMSs, the modulation exists only in the $c$-axis, i.e., $\mathbf{k} = (00\gamma)$ with $\gamma = c_{Mn}/c_{Si}$. From equation 1, both the $\mathbf{a_{s1}}$- and $\mathbf{a_{s2}}$-axes lie in the 3D physical space $\mathbf{R_3}$ and the $\mathbf{a_{s4}}$-axis is perpendicular to $\mathbf{R_3}$, as shown in Fig. 3. Similar to the unit bases, fractional coordinates in the (3+1)D space,

$\overline{x}_{s1}$, $\overline{x}_{s2}$, $\overline{x}_{s3}$ and $\overline{x}_{s4}$ can be defined as,

$$\begin{pmatrix} \overline{x}_{S1} \\ \overline{x}_{S2} \\ \overline{x}_{S3} \\ \overline{x}_{S4} \end{pmatrix} = \begin{pmatrix} 1 & 0 & 0 & 0 \\ 0 & 1 & 0 & 0 \\ 0 & 0 & 1 & 0 \\ \alpha & \beta & \gamma & 1 \end{pmatrix} \begin{pmatrix} \overline{x} \\ \overline{y} \\ \overline{z} \\ t \end{pmatrix} \tag{2}$$

where the parameter $t$, called as an internal coordinate, represents the distance from $\mathbf{R_3}$ and is related to the fourth coordinate $\overline{x}_{s4}$ by $\overline{x}_{s4} = \gamma\overline{z} + t$.

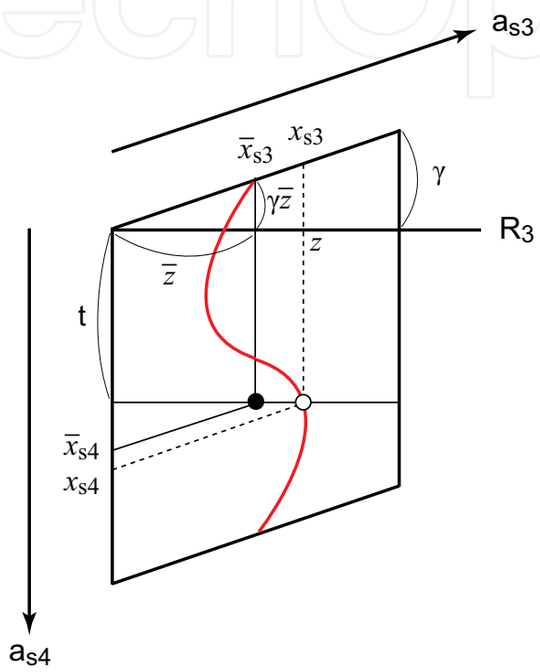


Fig. 3. A unit cell in the (3+1)-dimensional superspace and the relationship between the coordinates without modulation, $\overline{x}_{si}$, with modulation $x_{si}$ ($i$ = 1-4), and internal coordinate $t$. The red curve represents the positional modulation of an atom in subsystem 1. $\mathbf{R_3}$ denotes the 3D real space.

Due to the periodic difference along a particular direction, the composite crystals show positional (*displacive*) modulation of atomic sites. The positional modulation is periodic with an interval of $0 \leq \overline{x}_{s4} \leq 1$ as shown with the red curve in Fig. 3. The modulated position of an atom is then mathematically represented with a Fourier series as:

$$x_{si} = \overline{x}_{si} + \sum_{n=0}^{m} [A_n \cos(2\pi n \overline{x}_{s4}) + B_n \sin(2\pi n \overline{x}_{s4})], \tag{3}$$

where $i$ = 1,2,3.

### 2.3 Symmetry of HMSs

To specify the superspace group to the present HMSs, we need to consider an additional axis $c_{\mathrm{Si}}$ parallel to $c_{\mathrm{Mn}}$. The first subsystem [Mn] has a $\beta$-Sn type arrangement of Mn atoms

classified under the 3D space group of $I4_1/amd$. For the second subsystem [Si], originally having dimensions of $a/\sqrt{2} \times a/\sqrt{2} \times c_{Si}$, the $a$-axis length is adjusted to that of [Mn]. The Si atoms are at the origin and the equivalent positions generated by the $P4/nnc$ space group. According to Yamamoto (Yamamoto, 1993), the most appropriate (3+1)D superspace group is designated as $P : I4_1/amd : 1\bar{1}ss$ (Mn) $W : P4/nnc : q\bar{1}q1$ (Si), or based on the modulation vector $\mathbf{k} = (00\gamma)$ more conveniently as $I4_1/amd(00\gamma)00ss$.

Based on the adopted superspace group, the translation parts for the [Mn] subsystem are expressed as:
+(0, 0, 0, 0); +(1/2, 1/2, 1/2, 0),
with symmetry operations represented as:
(i) $x, y, z, t$;
(ii) $-y, x+1/2, z+1/4, t$;
(iii) $-x, y, z, t+1/2$;
(iv) $-x, -y, z, t$;
(v) $-y, -x+1/2, z+1/4, t+1/2$;
(vi) $y, -x+1/2, z+1/4, t$;
(vii) $x, -y, z, t+1/2$;
(viii) $y, x+1/2, z+1/4, t+1/2$;
(ix) $-x, -y+1/2, -z+1/4, -t$;
(x) $y, -x, -z, -t$;
(xi) $x, -y+1/2, -z+1/4, -t+1/2$;
(xii) $x, y+1/2, -z+1/4, -t$;
(xiii) $y, x, -z, -t+1/2$;
(xiv) $-y, x, -z, -t$;
(xv) $-x, y+1/2, -z+1/4, -t+1/2$;
(xvi) $-y, -x, -z, -t+1/2$.

The translation parts and the symmetry operation for the [Si] subsystem can be obtained by simply interchanging the third and the fourth components.

### 2.4 Structural modulation

Polycrystalline samples were prepared in a tetra-arc-type furnace under an Ar atmosphere using tungsten electrodes and a water-cooled copper hearth. Appropriate amounts of Mn (99.9%) and Si (99.99%) powders were mixed in an alumina mortar and pressed into pellets. The pellets were melted four times, and turned over each time to obtain full homogeneity. As the satellite reflections were observed up to eighth order in the electron diffraction patterns, positional modulation of the atomic sites was introduced taken to the eighth order of cosine and sine components of the Fourier terms, $A_n$ and $B_n$ ($n$= 0-8), of equation 3.

Figure 4 shows the observed, calculated, and difference profiles of the neutron diffraction (ND) data for $MnSi_\gamma$ at 295 K. The ND data were collected using a Kinken powder diffractometer for high efficiency and high resolution measurements, HERMES (Petricek et al., 2000), at the Institute for Materials Research (IMR), Tohoku University, installed at the JRR-3M reactor of the Japan Atomic Energy Agency (JAEA) at Tokai. A monochromatized incident neutron beam at $\lambda$ = 1.8265 Å was used. The ND data were analyzed with the JANA2000

software package (Petricek et al., 2000). The bound coherent scattering lengths used for the refinement were -3.730 fm (Mn) and 4.149 fm (Si).

The short vertical lines below the patterns indicate the peak positions of possible Bragg reflections. Small peaks at $2\theta \sim 32.5°$, 40.5°, and 53.0°, derived from the secondary phase MnSi, were excluded in the refinement cycles. The final $R$ factors were $R_{wp}$ = 9.8% and $R_p$ = 6.9%, and the lattice parameters were refined to $a$ = 5.5242(3) Å, $c_{Mn}$ = 4.3665(3) Å, and $c_{Si}$ = 2.5202(3) Å. The numbers in parentheses represent the estimated standard deviation of the last significant digit. The resulting $c$-axis ratio was $\gamma$ = 1.7326(1), different from that of any commensurate HMSs (Flieher et al., 1967; Gottlieb et al., 2003; Knott et al., 1967; Schwomma et al., 1963; 1964; Zwilling & Nowotny, 1973) and that for the sample annealed at 1273 K for 168 h from the same batch of the present sample of $\gamma$ = 1.7361(1) (Miyazaki, 2008).

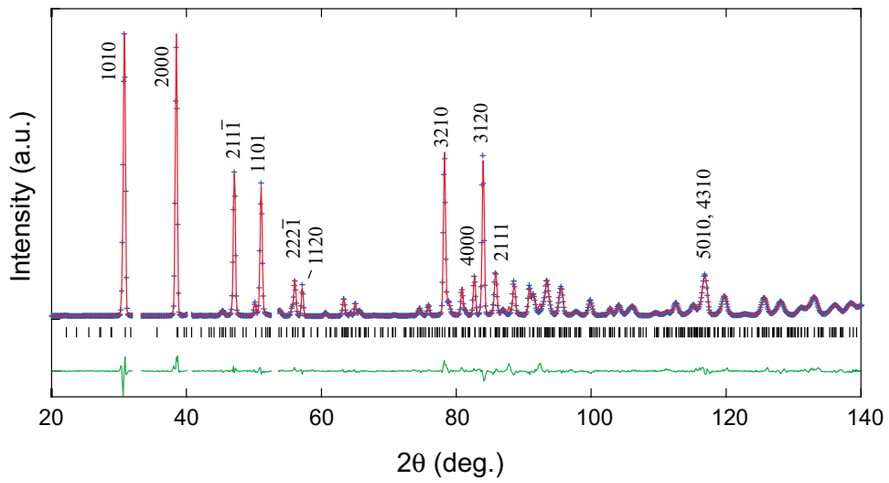


Fig. 4. Observed, calculated, and difference patterns of powder neutron diffraction data for $MnSi_\gamma$ measured at 295 K. Short vertical lines below the patterns indicate positions of Bragg reflections. The difference between the observed and calculated intensities is shown below the vertical lines. The peaks, denoted as $hkl0$ and $hk0m$, are the fundamental reflections derived from the [Mn] and [Si] subsystems, respectively, while the $hklm$ peaks are satellite reflections.

Table 1 summarizes the atomic coordinates and equivalent isotropic displacement parameters, $U_{eq}$, for the fundamental structure of $MnSi_\gamma$ at 295 K.

| Subsystem 1: [Mn] | $x$ | $y$ | $z$ | $U_{eq}$ (Å$^2$) |
|---|---|---|---|---|
| | 0 | 0 | 0 | 0.0057(12) |
| Subsystem 2: [Si] | $x$ | $y$ | $z$ | $U_{eq}$ (Å$^2$) |
| | 1/4 | 1/4 | 1/4 | 0.0139(12) |

Table 1. Atomic coordinates and equivalent isotropic atomic displacement parameters, $U_{eq}$, for the fundamental structure of $MnSi_\gamma$ at 295 K.

### 2.5 Details of modulated structure

Table 2 summarizes the refined Fourier amplitudes for the positional parameters together with the anisotropic displacement parameters of each atom. Due to the superspace group

symmetry, the number of refinable parameters of the Fourier terms is limited. Only even terms of the sine wave along the $z$-direction, i.e., $B_{2z}$, $B_{4z}$, $B_{6z}$, and $B_{8z}$, are allowed for the Mn atoms. In contrast, odd terms of the sine and cosine waves are allowed for both the $x$ and $y$ components for the Si atoms, along with $B_{4z}$ and $B_{8z}$ terms. The amplitudes of each cosine wave component in the $x$-$y$ plane, such as $A_{1x}$ and $A_{1y}$, are equal, whereas those of each sine wave are equal but their signs are opposite.

| Subsystem 1: [Mn] | $x$ | $y$ | $z$ |
|---|---|---|---|
| $B_2$ | 0 | 0 | -0.0142(12) |
| $B_4$ | 0 | 0 | 0.017(2) |
| $B_6$ | 0 | 0 | 0 |
| $B_8$ | 0 | 0 | 0 |
| $U_{11} = U_{22}$ = 0.002(2) (Å$^2$) | | | |
| $U_{33}$ = 0.013(2) (Å$^2$) | | | |
| **Subsystem 2: [Si]** | $x$ | $y$ | $z$ |
| $A_1$ | 0.0772(3) | = $A_{1x}$ | 0 |
| $B_1$ | = $A_{1x}$ | = -$A_{1x}$ | 0 |
| $A_3$ | 0.0103(3) | = $A_{3x}$ | 0 |
| $B_3$ | = -$A_{3x}$ | = $A_{3x}$ | 0 |
| $B_4$ | 0 | 0 | -0.0441(19) |
| $A_5$ | -0.0040(5) | = $A_{5x}$ | 0 |
| $B_5$ | = $A_{5x}$ | = -$A_{5x}$ | 0 |
| $A_7$ | -0.0034(7) | = $A_{7x}$ | 0 |
| $B_7$ | = -$A_{7x}$ | = $A_{7x}$ | 0 |
| $B_8$ | 0 | 0 | 0.017(4) |
| $U_{11} = U_{22}$ = 0.009(2) (Å$^2$) | | | |
| $U_{33}$ = 0.023(2) (Å$^2$) | | | |

Table 2. Refined positional modulation wave components and anisotropic displacement parameters, $U_{ij}$, for $MnSi_\gamma$.

In Fig. 5, we show the revealed positional modulations for the $x$, $y$, and $z$ coordinates of each atom plotted against $\overline{x}_{s4}$. The right vertical axes are re-scaled to represent the displacement (in Angstroms) for each atom. All the displacements are periodic in the interval $0 \leq \overline{x}_{s4} \leq 1$. For the Mn atoms, positional modulation is only allowed in the $z$ direction and the maximum displacement ($\sim$0.12 Å) from $z$ = 0 is recognized at $\overline{x}_{s4} \sim$ 0.18, 0.32, 0.68 and 0.82. The displacement of Si atoms along $z$ is comparable to that of the Mn atoms and the maximum displacement of ($\sim$0.13 Å) from $z$ = 1/4 can be seen at $\overline{x}_{s4} \sim$ 0.03, 0.19, 0.28, etc. Based on the large sine and cosine components, the rotational modulation in the $x$ and $y$ directions is significant for the Si atoms. Both the modulation waves in $x$ and $y$ are identical with the phase-shift of $\Delta\overline{x}_{s4}$ = 1/4. The maximum displacement of $\sim$0.54 Å from $x$ = 1/4, equivalent to $\Delta x \sim$ 0.1, is realized at $\overline{x}_{s4} \sim$ 0.48 and 0.98, and at $\overline{x}_{s4} \sim$ 0.23 and 0.73 from the $y$ = 1/4 position. Similar rotational modulations have been reported for related chimney-ladder compounds, such as $(Mo_{1-x}Rh_x)Ge_\gamma$ (Rohrer et al., 2000) and $(Cr_{1-x}Mo_x)Ge_\gamma$ (Rohrer et al., 2001). The deviation from the fundamental position, $\Delta x$ and $\Delta y$, is also $\sim$0.1 in these compounds, although the $a$-axis lengths of these phases ($a \sim$ 5.9 Å) are much larger than that in the present compound.

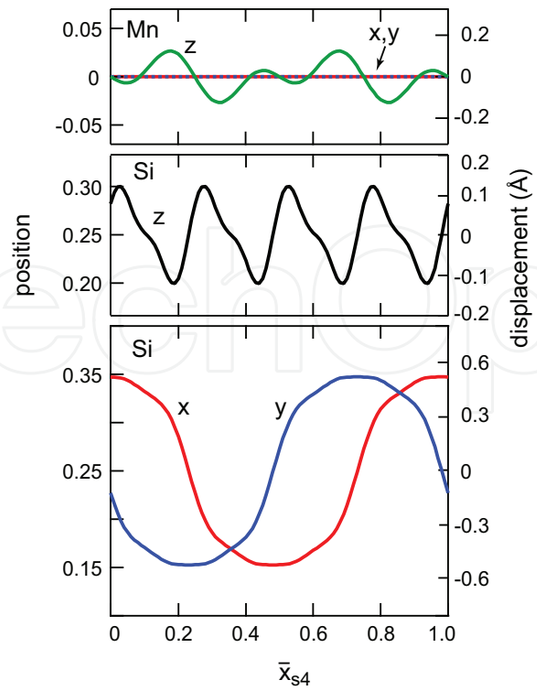


Fig. 5. Revealed positional modulations of the Mn and Si atoms plotted as a function of the fourth superspace coordinate, $\overline{x}_{s4}$. The right vertical axes are re-scaled to represent the displacement for each atom.

Figure 6 shows the revealed modulated structure of $MnSi_{\gamma}$ at 295 K. The top left figure illustrates the $c$-axis projection to represent the helical arrangement of the Si atoms. The bottom left figure depicts the atoms within a partial unit cell of length $4\times c_{Mn}$. The seven squares on the right represent slices of the 1st to 7th layers of Si atoms from the origin. The 1st layer of Si atoms corresponds to $\overline{x}_{s4} = (1/\gamma)(\overline{z} + t) = (1/\gamma)\times(1/4 - 1/4) = 0$, because the modulation vector component is inverted to $\gamma^{-1}$ for the [Si] subsystem. As deduced from Fig. 5, the coordinates at $\overline{x}_{s4} = 0$ are around $(x, y) = (0.35, 0.23)$. Since there is a two-fold axis at $(1/2, 1/2)$ parallel to the $c$-axis, the other Si atom in the 1st layer is located at around (0.65, 0.77). Similarly, the 3rd ($\overline{z} = 5/4$) and 5th ($\overline{z} = 9/4$) layers of Si atoms, corresponding to $\overline{x}_{s4} =$ 0.576 and 0.152 ($\equiv$ 1.152), are located at around (0.16, 0.32), (0.84, 0.68), and (0.32, 0.16), (0.68, 0.84), respectively. By symmetry, the coordinates of even numbered layers can be obtained as $(-x, y)$ and $(x, -y)$. The 2nd ($\overline{z} = 3/4$) and 4th ($\overline{z} = 7/4$) layers of Si atoms, corresponding to $\overline{x}_{s4} = 0.288$ and 0.864, are located at around (0.19, 0.85), (0.81, 0.15) and (0.33, 0.67), (0.67, 0.33), respectively. The $z$ coordinates of Si and Mn atoms in the modulated structure can also be calculated in a similar way.

Figure 7 shows interatomic distances plotted as a function of $t$. The two periodic curves around the distance of 3.0 Å represent the nearest four Mn-Mn distances, for which each curve is duplicated because of the two equidistant bonds. The nearest Mn-Mn distances, ranging from 2.92 Å to 3.01 Å, are relatively longer than that expected from the atomic radius of Mn, $r_{Mn}$ = 1.24 Å (Inoue et al., 2001). However, such long distances have been reported in the structure of $\alpha$-Mn (Bradley & Thewlis, 1927), wherein the Mn-Mn distances vary from 2.24 Å to 2.96 Å. In the case of the Mn-Si bonds, each Mn atom is coordinated to eight Si atoms, as deduced from Fig. 6. The four curves around 2.4 Å represent the nearest eight Mn-Si distances,

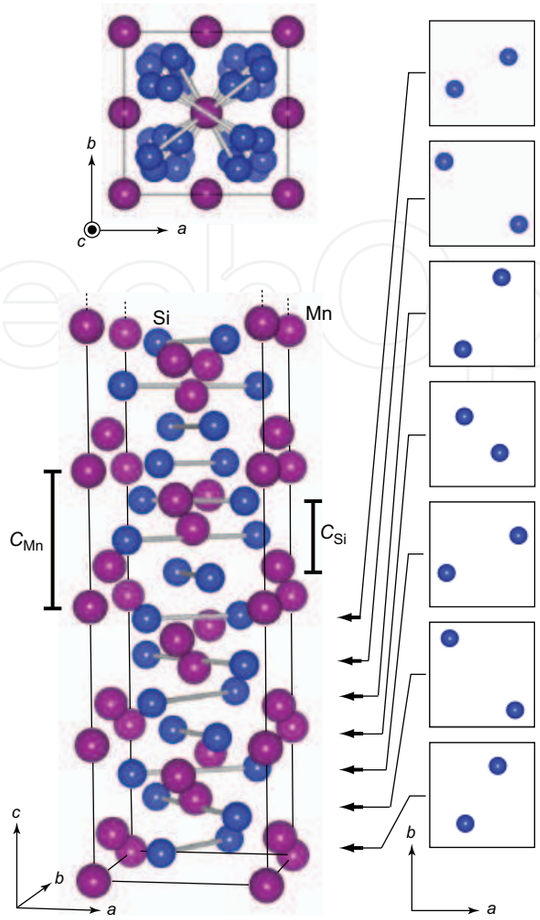


Fig. 6. Revealed modulated composite structure of $MnSi_\gamma$ at 295 K. The upper figure is a *c*-axis projection to illustrate the rotational arrangement of the Si atoms. The lower figure depicts the atoms within $4\times c_{Mn}$ lengths. The seven squares on the right are slices through the 1st to 7th layers of the Si subsystem from the origin.

with each curve duplicated due to equidistant Mn-Si bond pairs. At $t$ = 0, the Mn atom has eight Si neighbors with $d_{Mn-Si}\sim$ 2.4 Å, which is the typical Mn-Si bond distance on the basis of the metallic radii of Mn and Si ($r_{Si}$ = 1.17 Å) (Inoue et al., 2001). With increasing $t$, the four bonds (two curves) become shorter towards ∼2.2 Å, and the remaining four bonds become longer. In this way, the Mn atom is always bounded to eight Si atoms within a distance of $<$ 2.8 Å.

## 3. Universal treatment of HMSs by means of the superspace description

In principle, the superspace group approach described so far can also be applicable to *all* the reported commensurate structure of HMSs. Towards a uniform treatment of the crystal structure of the present $MnSi_\gamma$ and other HMSs, we will first convert the 3D coordinates of $Mn_4Si_7$ (Gottlieb et al., 2003) to $\overline{x}_{s4}$. The $Mn_4Si_7$ phase can be regarded as a case for which $\gamma$ = 7/4 = 1.75, wherein $4c_{Mn}$ exactly equals $7c_{Si}$; the 3D unit cell consists of a stacking of four [Mn] subsystems and seven intervening [Si] subsystems, as shown in Fig. 1. Let us consider the [Si] subsystem closest to the origin. The Si atom at Si1 (8*j*) sites with (0.15715, 0.2015, 0.11253) is

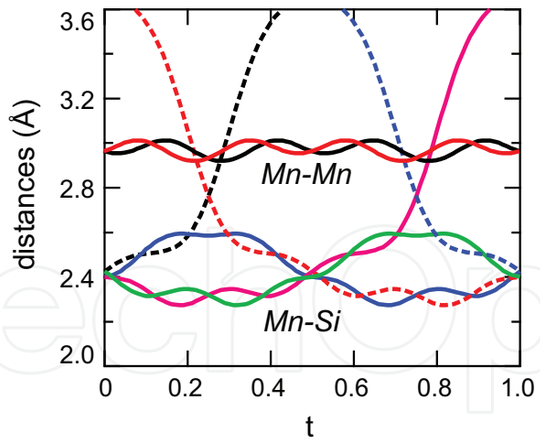


Fig. 7. Interatomic distances as a function of the internal coordinate $t$ for $MnSi_{\gamma}$ at 295 K.

converted to (0.15715, 0.2015, $\overline{z}+\delta$) in the [Si] subsystem. Since the Si atom is located at the 2nd ($\overline{z}$ = 3/4) layer, we obtain $\overline{x}_{s4} = (1/\gamma)\times(\overline{z} - 1/4) = 0.286$ and $3/4 + \delta = 7\times0.11253 = 0.788$.

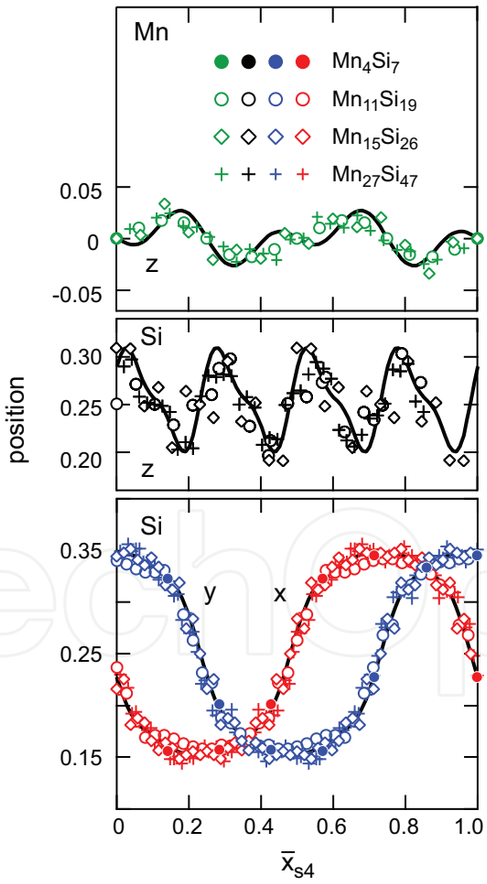


Fig. 8. The converted coordinates of Mn at ~ (0, 0, 0) and Si at ~ (1/4, 1/4, 1/4) in each subsystem of HMSs plotted as a function of the superspace coordinate, $\overline{x}_{s4}$. Solid lines are the data of the present incommensurate $MnSi_{\gamma}$ ($\gamma$ = 1.7326(1)).

Similarly, the Si atom at Si4 ($8j$) sites with (0.34518, 0.2274, 0.9620) is converted to (0.34518, 0.2274, $27/4+\delta'$) with $\overline{x}_{s4} = 0.714$ ($\equiv 3.714$). In this case, $27/4 + \delta'$ equals $7\times0.9620 = 6.734$ in the [Si] subsystem, corresponding to $z = 0.734$ in the 7th [Si] subsystem from the origin. By applying all the symmetry operations to the Mn1-Mn5 and Si1-Si4 sites, the equivalent positions close to Mn (0, 0, 0) and Si (1/4, 1/4, 1/4) in each subsystem can be obtained as filled circles shown in Fig. 8.

Based on this structuring, those equivalent positions as a function of $\overline{x}_{s4}$ of $Mn_{11}Si_{19}$ ($\gamma = 1.7\dot{2}\dot{7}$) (Schwomma et al., 1963; 1964), $Mn_{15}Si_{26}$($\gamma = 1.7\dot{3}$) (Flieher et al., 1967; Knott et al., 1967) and $Mn_{27}Si_{47}$($\gamma = 1.7\dot{4}\dot{0}\dot{7}$) (Zwilling & Nowotny, 1973) are converted into the respective marks as shown in Fig. 8. The solid lines in these panels correspond to those shown in Fig. 5 but the $x$ and $y$ lines are interchanged to preserve the original ($x$, $y$) coordinates given in the reports (Flieher et al., 1967; Gottlieb et al., 2003; Knott et al., 1967; Schwomma et al., 1963; 1964; Zwilling & Nowotny, 1973). All the $x$ and $y$ coordinates of the points in the [Si] subsystem are well superposed on the two *universal* lines, suggesting that the helical arrangement of Si atoms is almost identical and independent of the $\gamma$ values in all HMSs. In contrast, the $z$ coordinates for the Mn and Si atoms deviate from the periodic solid lines of the present sample. It would be, however, reasonable to consider different shape of curves, i.e., different $B_z$ terms, to fit the $z$ coordinates for each HMS because the stacking periodicity might be dependent on $\gamma$.

## 4. Conclusion

A superspace group approach is economical in describing an incommensurate compound by using a much reduced number of parameters. The positional modulation of the atoms can be expressed by means of a Fourier expansion of the modulation functions. For HMSs, both the Mn and Si atoms are at special positions in each subsystem and their modulated positions are excellently described by only *eight* parameters. This is much smaller set compared with other HMSs with a 3D description; the number of refinable positional parameters are 13 ($Mn_4Si_7$), 41 ($Mn_{11}Si_{19}$), 26 ($Mn_{15}Si_{26}$) and 97 ($Mn_{27}Si_{47}$). These four phases have different 3D symmetries and lattice parameters but by using the superspace group approach, we can treat these phases as an identical compound $MnSi_\gamma$, with slightly different stoichiometric $\gamma$ values. Moreover, this approach affords a uniform treatment of a compound system which can change its stoichiometry incommensurately upon substitution of the elements. For example, a partial substitution of Cr, Fe, and Co is possible at Mn sites and such a solid solution can also be simply represented as $(Mn_{1-x}M_x)Si_\gamma$ ($M$ = Cr, Fe and Co) (Flieher et al., 1967). Ranging over the various solid solutions, the $\gamma$ value is known to change from 1.65 through 1.76. The next target should be to optimize the TE properties by tuning the electronic structure of HMSs and we hope that these TE materials can be prepared in the present HMS-based compounds in the near future.

## 5. References

Bradley, A. J. & Thewlis, J. (1927). The crystal structure of $\alpha$-manganese. *Proc. Royal Soc. London, Ser. A* 115: 456-471, 0080-4630.

De Wolff, P. M. (1974). The pseudo-symmetry of modulated crystal structures. *Acta Cryst.* A30: 777-785, 0567-7394.

Fedorov, M. I. & Zaitsev, V. K. (2006). Thermoelectrics of transition metal silicides, In: *Thermoelectrics Handbook Macro to Nano*, Rowe, D. M., (Ed.), chap.31, CRC press, Boca Raton, 0-8493-2264-2, London.

Flieher, G.; Vollenkle, H.; Nowotny, H. (1967). Die Kristallstruktur von $Mn_{15}Si_{26}$, *Monatsh. Chem.* 98: 2173-2179, 0026-9247.

Gottlieb, U.; Sulpice, A.; Lambert-Andron, B.; Laborde, O. (2003). Magnetic Properties of Single Crystalline $Mn_4Si_7$, *J. Alloys Compd.* 361: 13-18, 0925-8388.

Inoue, T.; Chikazumi, S.; Nagasaki, S; Tanuma, S. (2001). *Agne Periodic Table*, AGNE Technology Center, 978-4-901496-37-7,Tokyo.

Janner, A. & Janssen, T. (1980). Symmetry of incommensurate crystal phases. II. Incommensurate basic structure, *Acta Cryst.* A36: 408-415, 0567-7394.

Knott, H. W.; Mueller, M. H.; Heaton, L. (1967). The Crystal Structure of $Mn_{15}Si_{26}$, *Acta Cryst.* 23: 549-555, 0365-110X.

Miyazaki, Y.; Igarashi, D.; Hayashi, K.; Kajitani, T.; Yubuta, K. (20080. Modulated Crystal Structure of Chimney-Ladder Higher Manganese Silicides $MnSi_\gamma$ ($\gamma\sim$ 1.74), *Phys. Rev. B* 78, 214104 (8 pages), 1098-0121.

Momma, K. & Izumi, F. (2008). VESTA: a three-dimensional visualization system for electronic and structural analysis. *J. Appl. Cryst.* 41: 653-658, 0021-8898.

Nikitin, E. N.; Tarasov, V. I.; Tamarin, P. V. (1969). Thermal and electrical properties of the higher manganese silicide from 4.2 to 1300 K and its structure, *Sov. Phys. Solid State* 11: 187-189, 0038-5654.

Nishida, I. (1973). Semiconducting properties of nonstoichiometric manganese silicides. *J. Mater. Sci.* 7: 435-440, 0022-2461.

Ohoyama, K.; Kanouchi, T.; Nemoto, K.; Ohashi, M.; Kajitani, T.; Yamaguchi, Y. (1998). The new neutron powder diffractometer with a multi-detector system for high-efficiency and high-resolution measurements, *Jpn. J. Appl. Phys.* 37: 3319-3326, 0021-4922.

Okamoto, H. (1991). Mn-Si (Manganese-Silicon), *J. Phase Equilibria* 12: 505-507, 1054-9714.

Petricek, V.; Dusek, M.; Palatinus, L. (2000). *JANA2000 The crystallographic computing system*. Institute of Physics, Praha, Czech Republic.

Rohrer, F. E.; Lind, H.; Eriksson, L.; Larsson, A. K.; Lidin, S. (2000). One the question of commensurability - The Nowotny chimney-ladder structures revisited. *Z. Kristallogr.* 215: 650-660, 1433-7266.

Rohrer, F. E.; Lind, H.; Eriksson, L.; Larsson, A. K.; Lidin, S. (2001). Incommensurately modulated Nowotny Chimney-ladder phases: $Cr_{1-x}Mo_xGe_{\sim 1.75}$ with $x$ = 0.65 and 0.84. *Z. Kristallogr.* 216: 190-198, 1433-7266.

Schwomma, O.; Nowotny, H.; Wittmann, A. (1963). Die Kristallarten $RuSi_{1.5}$, $RuGe_{1.5}$ und $MnSi_{\sim 1.7}$, *Monatsh. Chem.* 94: 681-685, 0026-9247.

Schwomma, O.; Preisinger, A.; Nowotny, H.; Wittmann, A. (1964) Die Kristallstruktur von $Mn_{11}Si_{19}$ und deren Zusammenhang mit Disilicid-Typen, *Monatsh. Chem.* 95: 1527-1537, 0026-9247.

Terasaki, I. (2003). Thermoelectric cobalt oxides. *Parity* 64-67 (*in Japanese*).

Yamamoto, A. (1993). Determination of Composite Crystal Structures and Superspace Groups, *Acta Cryst. A* 49: 831-846, 0567-7394.

Ye, H. Q. & Amelinckx, S. (1986). High-Resolution Electron Microscopic Study of Manganese Silicides $MnSi_{2-x}$, *J. Solid State Chem.* 61: 8-39, 0022-4596.

Zwilling, G. & Nowotny, H. (1973). Zur Struktur der Defekt-Mangansilicide, *Monatsh. Chem.* 104: 668-675, 0026-9247.

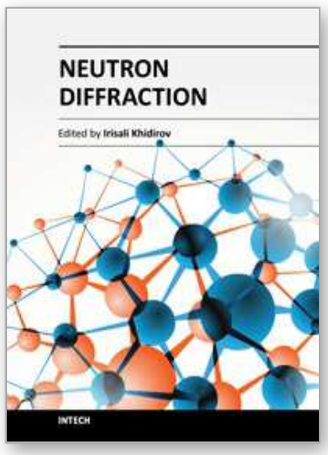


**Neutron Diffraction**

Edited by Prof. Irisali Khidirov

ISBN 978-953-51-0307-3
Hard cover, 286 pages
**Publisher** InTech
**Published online** 14, March, 2012
**Published in print edition** March, 2012

Now neutron diffraction is widely applied for the research of crystal, magnetic structure and internal stress of crystalline materials of various classes, including nanocrystalls. In the present book, we make practically short excursion to modern state of neutron diffraction researches of crystal materials of various classes. The book contains a helpful information on a modern state of neutron diffraction researches of crystals for the broad specialists interested in studying crystals and purposeful regulation of their service characteristics, since the crystal structure, basically, defines their physical and mechanical properties. Some chapters of the book have methodical character that can be useful to scientists, interested in possibilities of neutron diffraction. We hope, that results of last years presented in the book, can be a push to new ideas in studying of crystalline, magnetic structure and a macrostructure of usual crystal materials and nanocrystals. In turn, it can promote working out of new materials with new improved service characteristics and to origin of innovative ideas.

**How to reference**

In order to correctly reference this scholarly work, feel free to copy and paste the following:

Yuzuru Miyazaki (2012). Superspace Group Approach to the Crystal Structure of Thermoelectric Higher Manganese Silicides MnSi , Neutron Diffraction, Prof. Irisali Khidirov (Ed.), ISBN: 978-953-51-0307-3, InTech, Available from: http://www.intechopen.com/books/neutron-diffraction/superspace-group-approach-to-the-crystal-structure-of-thermoelectric-higher-manganese-silicides-mnsi

INTECH
open science | open minds

**InTech Europe**
University Campus STeP Ri
Slavka Krautzeka 83/A
51000 Rijeka, Croatia
Phone: +385 (51) 770 447
Fax: +385 (51) 686 166
www.intechopen.com

**InTech China**
Unit 405, Office Block, Hotel Equatorial Shanghai
No.65, Yan An Road (West), Shanghai, 200040, China
中国上海市延安西路65号上海国际贵都大饭店办公楼405单元
Phone: +86-21-62489820
Fax: +86-21-62489821

IntechOpen